mation is inherently weak (Popper, 1959 (*19*)]. For a recent perspective on probabilistic confirmation, see A. Franklin and C. Howson, *Stud. Hist. Philos. Sci.* **19**, 419 (1988); and C. Howson and P. Urbach, *Scientific Reasoning: The Bayesian Approach* (Open Court, La Salle, IL, 1989).
40. Carnap therefore argued that all inductive logic was a logic of probability [R. Carnap, in *The Problem of Inductive Logic*, I. Lakatos, Ed. (North Holland, Amsterdam, 1968), pp. 258–267]. Confirming observations give us warrant for a certain degree of belief.
41. An example is the evidence of faunal homologies in Africa and South America, before the acceptance of plate tectonic theory. These data, which were used as an early argument in favor of continental drift, were considered to be equally well explained by the hypothesis of land bridges [N. Oreskes, *Hist. Stud. Phys. Sci.* **18**, 311 (1988)].
42. An obvious example of this is Ptolemaic astronomy, which was extremely well confirmed for centuries and then overturned completely by the Copernican revolution. See T. S. Kuhn, *The Copernican Revolution* (Harvard Univ. Press, Cambridge, MA, 1957). Indeed, every scientific revolution involves the overturning of well-confirmed theory. See I. B. Cohen, *Revolution in Science* (Belknap Press, Cambridge, MA, 1985).
43. Konikow and Bredehoeft (*2*), on the basis of their extensive experience with both scientists and government officials, emphasize that the language of verified and validated models is typically interpreted to mean that the models under discussion are, in essence, true. It is also clear that this is the intent of many authors who claim to base results on "validated" models.
44. We have never seen a paper in which the authors wrote, "the empirical data invalidate this model."
45. Another example is found in the environmental assessment overview for Yucca Mountain (*29*, p. 4). The task of site selection, as defined in this report, consisted of "evaluat[ing] the potentially acceptable sites against the disqualifying conditions. . . ." The authors concluded that the Yucca Mountain site was "not disqualified." That is, the null hypothesis is that the site is safe; the burden of proof is on those who would argue otherwise.
46. N. Cartwright, *How the Laws of Physics Lie* (Clarendon Press, Oxford, 1983), p. 153.
47. This article was prepared for a session on hydrological and geochemical modeling in honor of David Crerar at the American Geophysical Union, May 1993. We thank the organizers, A. Maest and D. K. Nordstrom, for inviting us to prepare this article; J. H. Fetzer, L. Konikow, M. Mitchell, K. Nordstrom, L. Sonder, C. Drake, and two reviewers for helpful comments on the manuscript; and our research assistant, D. Kaiser. We dedicate this paper in appreciation of the work of David Crerar.

RESEARCH ARTICLE

Routes to Catalysis: Structure of a Catalytic Antibody and Comparison with Its Natural Counterpart

Matthew R. Haynes, Enrico A. Stura, Donald Hilvert, Ian A. Wilson

The three-dimensional structure of a catalytic antibody (1F7) with chorismate mutase activity has been determined to 3.0 Å resolution as a complex with a transition state analog. The structural data suggest that the antibody stabilizes the same conformationally restricted pericyclic transition state as occurs in the uncatalyzed reaction. Overall shape and charge complementarity between the combining site and the transition state analog dictate preferential binding of the correct substrate enantiomer in a conformation appropriate for reaction. Comparison with the structure of a chorismate mutase enzyme indicates an overall similarity between the catalytic mechanism employed by the two proteins. Differences in the number of specific interactions available for restricting the rotational degrees of freedom in the transition state, and the lack of multiple electrostatic interactions that might stabilize charge separation in this highly polarized metastable species, are likely to account for the observed 10^4 times lower activity of the antibody relative to that of the natural enzymes that catalyze this reaction. The structure of the 1F7 Fab′-hapten complex provides confirmation that the properties of an antibody catalyst faithfully reflect the design of the transition state analog.

The mammalian immune system has been successfully exploited by chemists to create antibody molecules with tailored catalytic activities and specificities. Haptens designed to mimic the key stereoelectronic features of transition states can induce antibodies capable of catalyzing various chemical transformations, ranging from simple hydrolyses to reactions that lack physiological counterparts or are normally disfavored (*1*). The ability to create novel active sites in this way (*2*) permits systematic exploration of the basic principles of biological catalysis and, through comparison with naturally occurring enzymes, evaluation of alternative catalytic pathways for particular reactions. In the absence of structural information, it is difficult to determine precisely the extent to which the transition state analog dictates the catalytic characteristics of the induced antibody. Thus, detailed knowledge of the mode of transition state analog binding by antibodies should facilitate the further development, through rational redesign, of both transition state analogs and first-generation catalytic antibodies.

The unimolecular conversion of (−)-chorismate into prephenate (Fig. 1) was one of the first nonhydrolytic reactions to be catalyzed by an antibody (*3*, *4*). This concerted transformation, formally a Claisen rearrangement, has been intensively studied as a rare example of a biologically relevant pericyclic reaction (*5*–*11*). In microorganisms and higher plants prephenate production is the committed step in the biosynthesis of tyrosine and phenylalanine, and the enzyme chorismate mutase accelerates this reaction by more than 2 million. Although the precise factors that contribute to the efficiency of the enzyme are still poorly understood, it is known that the uncatalyzed reaction occurs through an asymmetric chairlike transition state **2** in which carbon-oxygen bond cleavage precedes carbon-carbon bond formation (*7*, *8*). In aqueous solution the flexible chorismate molecule preferentially adopts the extended pseudodiequatorial conformation **1a** and must be converted to the higher energy pseudo-diaxial conformer **1b** on the way to the transition state (*9*). Binding sites that are complementary to the compact transition state species (and the corresponding substrate conformer) would therefore be expected to increase substantially the probability of reaction. The favorable entropy of activation ($\Delta\Delta S^{\ddagger} = 13$ cal K^{-1} mol^{-1}) of the enzyme-catalyzed process compared to the spontaneous thermal rearrangement is consistent with this idea (*6*), as is the observation of strong enzyme inhibition by the conformationally restricted *endo*-oxabicyclic dicarboxylic acid **4** which approximates the structure of **2** (*12*). Stabilization of any charge separation in the transition state through electrostatic or hydrogen bonding interactions might also contribute to the potency of the enzyme (*13*).

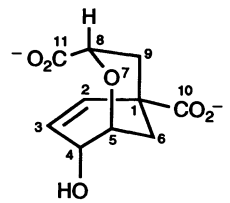

4

M. R. Haynes, E. A. Stura, and I. A. Wilson are in the Department of Molecular Biology, The Scripps Research Institute, La Jolla, CA 92037. D. Hilvert is with the Departments of Chemistry and Molecular Biology, The Scripps Research Institute, La Jolla, CA 92037.

Inhibitor **4** was used independently in two different laboratories as the template for generating antibodies with chorismate mutase activity (*3*, *4*). In each case, this transition state analog was linked to a carrier protein for immunization through its nonessential (*14*) C-4 hydroxyl group, leaving the two negatively charged carboxylate groups as the primary determinants for immune recognition. The resulting antibodies accelerated the enantioselective rearrangement of chorismate with rate enhancements in the range 10^2 to 10^4 over background, or in the best case only about two orders of magnitude less than that achieved by the enzyme. Like chorismate mutase, the more active of these catalysts (11F1-2E9) significantly lowers the entropy barrier for the rearrangement ($\Delta\Delta S^{\ddagger}$ = 11 cal K^{-1} mol^{-1}) (*4*), suggesting that it effectively restricts the conformational freedom of the bound substrate molecule. In contrast, the catalytic effects exhibited by antibody 1F7 ($k_{cat}/k_{un} \approx 200$) result entirely from a lowering of the enthalpic barrier; the entropy of activation in this case is considerably less favorable than for the uncatalyzed reaction ($\Delta\Delta S^{\ddagger} = -9$ cal K^{-1} mol^{-1}) (*3*). Because 1F7 preferentially binds a diaxial conformer of chorismate, as judged by diagnostic intramolecular transferred nuclear Overhauser effects (*15*), the unfavorable entropic change that accompanies this antibody-catalyzed reaction may reflect protein conformational changes or desolvation of the substrate or binding site (or both). In any case, the distinctive kinetic and thermodynamic properties of 1F7 and 11F1-2E9 provide a good example of the diversity available from the immune system.

Comparison of the structural features of these catalytic antibodies with those of the corresponding natural enzymes could provide broad insight into the range of catalytic effects and the specific chemical mechanisms that can be exploited by proteins to enhance the rate of this reaction. Here we report the crystal structure of 1F7 complexed with the transition state analog **4** and compare it to the recently reported structure of a monofunctional chorismate mutase from *Bacillus subtilis* complexed with the same transition state analog (*16*).

Crystallization and data collection. The complex formed by the Fab′ fragment of 1F7 and the transition state analog was crystallized as described (*17*). Briefly, the immunoglobulin (IgG1,κ) was isolated from mouse ascites fluid and cleaved with pepsin to yield the $F(ab')_2$ fragment, and subsequently reduced with cysteine to produce Fab′. After fast protein liquid chromatography purification, the Fab′ fragment was crystallized in the presence of the transition state analog **4**. Crystals of the complex were grown in sitting drops, by the vapor diffusion method, from 1.62 M ammonium sulfate, 0.06 M Pipes, pH 7.25, at 22.5°C. The concentrations of Fab′ and hapten were approximately 1 mM and 5 mM, respectively. The crystals thus obtained were extremely thin plates with maximum dimensions of about 0.50 by 0.04 by 0.01 mm. The small size of the crystals places an inherent limit on the intensity of the diffracted radiation, necessitating long times for data frame collection (up to 15 minutes) and reducing the signal-to-noise ratio of the data (Table 1).

Structure determination. The structure of the 1F7 Fab′-hapten complex was determined to 3.0 Å resolution by molecular replacement. Rotation functions of various Fab models were analyzed with MERLOT (*18*). The cleanest solution for an intact Fab model (four domains) was obtained with the phosphocholine-binding antibody McPC603 (the second peak height was 79.5 percent of the first peak value), although similar rotation solutions were observed for other models with similar elbow angles. This solution was confirmed by Patterson correlation (PC) refinement with X-PLOR (*19*). The rotation solution selected with MERLOT produced the highest PC value (the second peak height was 61 percent of the first peak value). The rotated and PC-refined model was then subjected to a translation function search by an implementation of the Harada translation function (*20*). The translation solution was likewise unambiguous, with the second peak height at 72 percent of the first peak value. After rigid body refinement of the model with X-PLOR, to adjust the relative positions of the four Fab′ domains (V_H, V_L, C_H1, C_L) as independent units, the crystallographic *R* value was 45 percent.

At this point the variable and constant domains of the antibody to lysozyme (HyHEL-5) were superimposed independently on the corresponding domains of McPC603. The HyHEL-5 antibody has a higher sequence similarity (≈80 percent identity) with 1F7, and its separate variable and constant domains gave cleaner rotation function solutions than did the variable and constant domains of McPC603. The procedure thus produced a model from the variable and constant domains of HyHEL-5 but with the elbow angle of McPC603 (133.2°). Rigid body and least-squares positional refinement of this model lowered the *R* values to 41 and 25 percent, respectively. The amino acid residues of the model which differed from those of 1F7 were truncated to alanines in the initial stages of refinement. The structure was refined by multiple cycles of X-PLOR least-squares refinement and simulated annealing, and manual building with FRODO (*21*). The truncated residues were built into the model using 10 percent F_0-F_c omit electron density maps to reduce model bias (*22*). After several refinement cycles, electron density for the hapten in the antibody binding site was clearly evident from F_0-F_c maps. The transition state analog was placed into this density in several trial orientations, as the moderate resolution of the data and the small size of the analog raised the possibility of some uncertainty in its precise position. In fact, the correct choice of orientation was unambiguous, as it resulted in far superior electron density for the transition state analog in F_0-F_c omit maps, following least-squares refinement and simulated an-

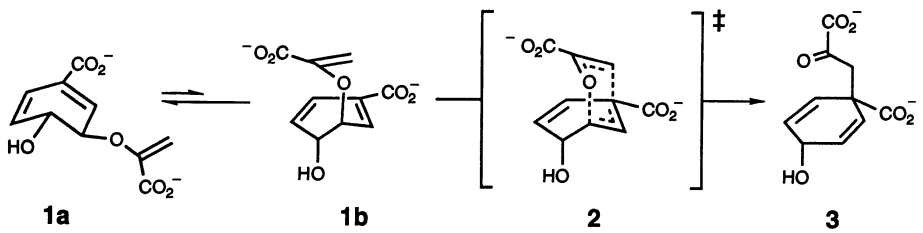

Fig. 1. The Claisen rearrangement of (−)-chorismate [**1**] to form prephenate **3**. Inhibitor **4** mimics the structure of the conformationally restricted transition state [**2**] and was used to elicit antibodies 1F7 (*3*) and 11F1-2E9 (*4*).

Table 1. Data collection and refinement statistics for the 1F7-hapten structure. The crystals belong to the orthorhombic space group $P2_12_12_1$, with unit cell dimensions a = 37.1 Å, b = 63.3 Å, and c = 178.5 Å. The Matthews constant (*36*) V_m is 2.10 Å³/Da, and the solvent content of the crystals is 41 percent with one Fab′-hapten complex per asymmetric unit. Data were collected at room temperature, with an Elliott GX-18 rotating anode x-ray generator operating at 40 kV, 55 mA, Franks focusing mirrors (*37*), and a Siemens multiwire area detector. Diffraction data recorded from two crystals were merged and scaled by means of XENGEN (*38*).

Number of observations	19,033
Number of unique reflections	8,660
Completeness to max. resolution (%)	95.8
Completeness, 3.4 to 3.0 Å range (%)	91.7
$R_{sym}(I)$ (%)	8.6
Average I/σ	4.4
Refinement resolution (Å)	12 to 3.0
R_{cryst} (%)	22
rms Δ bond lengths (Å)	0.017
rms Δ bond angles (degrees)	4.06
rms Δ dihedrals (degrees)	27.5
rms Δ impropers (degrees)	2.00

nealing (Fig. 2). The relative thermal parameters for the hapten atoms were also consistently lower for this orientation than for all others investigated, increasing the level of confidence in this positioning of the hapten.

The quality of the electron density maps was poorer in some external loops of the protein, resulting in less favorable geometry for a few residues. However, an analysis with the program PROCHECK (*23*) indicates that the overall stereochemical quality of the structure is better than average in comparison with other structures at the same resolution, with 70.8 percent of the residues in "most favored" regions of the Ramachandran plot, and 97.8 percent in allowed regions. Those residues that lie in disfavored regions (8 out of 431) are generally confined to surface loops that are relatively distant from the hapten. In addition to the main-chain geometry, the analysis shows that the 1F7-hapten complex structure is better than average for its resolution in terms of nonbonded interactions, hydrogen bond energies, and side-chain chi angles. Luzzati analysis (*24*) suggests that the coordinate error of the model is approximately 0.30 to 0.50 Å, which is sufficient to establish the orientation of the hapten and its disposition with respect to the antibody side chains.

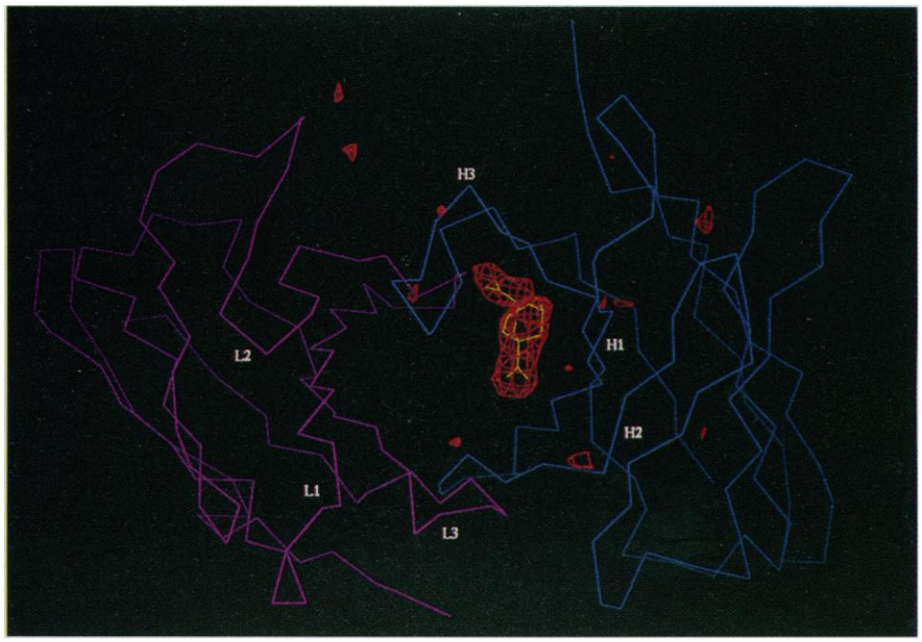

Fig. 2. An F_o-F_c omit electron density map of the transition state analog at 3.0 Å resolution, contoured at 3.0 σ. The density (red) for the transition state analog (yellow) is the only significant feature, as can be seen from the superposition of the map on the Fab′ structure. The view is into the antibody combining site and shows the light chain in red and the heavy chain in blue. The close association of the hapten with the heavy chain, particularly CDR-H3, is clearly seen. The complementarity determining regions (CDRs) or hypervariable loops are labeled L1-L3 (light chain) and H1-H3 (heavy chain).

Structure analysis. The Fab′ structure shows overall similarity to other known antibody structures. The transition state analog is bound at the apex of the variable domain by the complementarity determining regions (CDRs), which are the tips of six loops from the heavy (H1 to H3) and from the light (L1 to L3) chains (Fig. 2). An unusual feature of the 1F7 Fab′ structure is the relatively flat CDR surface with minimal loop protrusion (Fig. 3). This arrangement has been generally associated with antibodies generated against proteins and contrasts with the concave bowl-like or cleft topology often found in antibodies that bind small haptens (*25*). The comparative flatness of the CDR region is unlikely to influence catalytic activity, as the hapten binds in a small pocket in this surface and is almost completely enveloped by the surrounding protein residues (Fig. 4).

Analysis of the combining site of 1F7 (Figs. 5 and 6A) illustrates that a combination of hydrophobic, electrostatic, and hydrogen-bonding interactions mediates hapten recognition. Overall, the contact areas and type of antibody-hapten interactions observed in the complex are comparable to those in complexes of other antibodies with haptens of a similar size and are generally intermediate between the values reported for the McPC603-phosphocholine complex and the Fab 4-4-20 bound to fluorescein (*25*, *26*). The hapten interacts primarily with the heavy chain (V_H), contacting CDRs H1 (two residues), H2 (one residue), and H3 (four residues). The light chain contacts the transition state analog only through a single side chain of an L3 residue. This preferential utilization of the heavy chain CDRs is consistent with most other complexed Fab structures, particularly in cases of antibodies to small molecules (*26*), but 1F7 represents an extreme case. Good (albeit imperfect) shape complementarity between the Fab and the transition state analog is indicated from the 182 Å^2 of the hapten (roughly 90 percent of the total solvent-accessible surface) and the 265 Å^2 of the Fab′ surface that become buried in the complex (*27*). Nearly 90 percent of the total antibody surface area buried by the hapten is contributed by the heavy chain variable domain, and 62 percent is from CDR H3 alone.

There are 37 van der Waals contacts and three hydrogen bonds between the transition state analog and the antibody. Most (17 of 21) of the antibody atoms in direct contact with the hapten belong to the side chains of the protein. The floor of the binding site is formed by the side chains of Asn^{H35}, Trp^{H47}, Ala^{H93}, Phe^{H100b}, and Leu^{L96}, which provide a relatively hydrophobic base for the cavity. Residues with polar side chains make up the walls of the binding site and include Asn^{H33}, Asn^{H50},

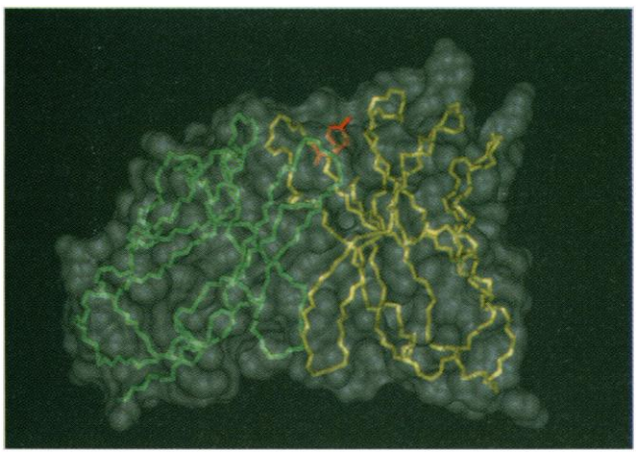

Fig. 3. Solvent-accessible surface of the 1F7 variable domain (1.7 Å sphere radius), showing the location of the hapten (red) buried in the combining site. The light chain (Cα trace) is on the left in green and the heavy chain is on the right in yellow. The transition state analog can be seen in a small indentation in the otherwise flat surface of the combining site (*39*).

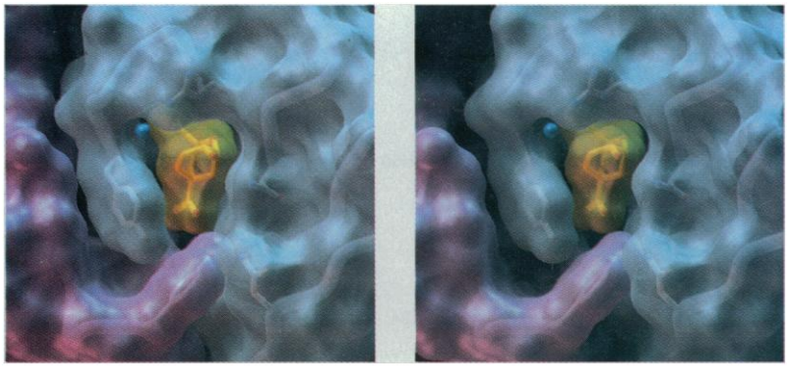

Fig. 4. Stereoview of the 1F7 Fab' binding site, with separate solvent-accessible surfaces (1.7 Å sphere radius) shown for the light chain, heavy chain, and the hapten. The view is the same as in Fig. 2, and reveals the complementarity of the binding site to the transition state analog. The relatively open space around the C-11 carboxyl group is apparently filled with a bound water molecule (blue sphere) that provides a bridge between the hapten and the antibody and increases the complementarity of fit (*29*). The OH group through which the hapten was attached to the carrier protein protrudes into the solvent as expected (*40*).

Asn^{H58}, Arg^{H95}, Tyr^{H100}, and Tyr^{L94}. In the case of Tyr^{H100}, only the aromatic ring is in van der Waals contact with the hapten's cyclohexenyl ring; the phenolic group is not positioned appropriately to contribute a hydrogen bond to any polar functionality of the hapten.

Although racemic hapten was used for the crystallization experiments, only a single enantiomer is observed bound at the active site. The antibody complementarity to the structural isomer 4 that has the same stereochemical relationships among functional groups as (−)-chorismate provides a compelling structural basis for the enantioselectivity observed for 1F7 (*3*). Consistent with the way in which the hapten was originally attached to its carrier protein for immunization, the C-4 hydroxyl group is located at the mouth of the pocket. While this group is largely solvent exposed, it participates in a hydrogen bond (either as an acceptor or a donor) with the side chain of Asn^{H33}, which could contribute both to the affinity and specificity of the antibody binding site for the transition state analog.

Orientation of the transition state analog within the pocket appears to be dictated primarily by specific interactions with the two carboxylate groups. The C-10 carboxylate is fixed in place through a hydrogen bond with the phenolic group of Tyr^{L94}. Otherwise, no formal positive charge is present at this site in the pocket to neutralize the negative charge, but an extensive hydrogen-bonding network among the side-chains of Tyr^{L94}, Asn^{H35}, Trp^{H47}, Asn^{H50}, and Asn^{H58} may help to distribute the charge in a manner analogous to that seen in some structures of peptide-complexed antibodies (*28*). The C-11 carboxylate group, on the other hand, is the most buried part of the hapten. It appears to form a hydrogen bond to a putative water molecule that is in turn hydrogen bonded to the backbone carbonyl oxygen of Asp^{H97} (*29*). The side chain of Arg^{H95} (CDR H3) lies above the C-11 carboxylate in a position that also places it near the transition state analog ether oxygen. In addition to providing the expected electrostatic complementarity to this portion of the hapten, this residue partially shields the ligand from solvent. Consequently, dissociation of the transition state analog from the binding pocket may require a substantial conformational rearrangement of the Arg^{H95} side chain. Although the active site contains only a single formal positive charge, there are other basic residues nearby (His^{H32}, Arg^{H94}, and Arg^{H96}) that may contribute to overall charge complementarity within the complex.

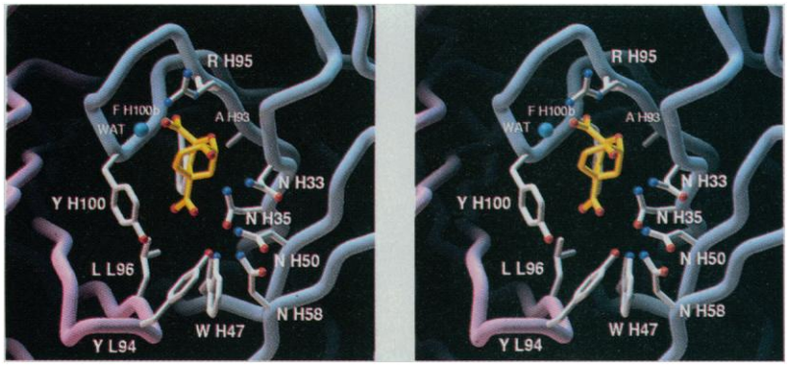

Fig. 5. Stereoview of the 1F7 Fab' binding site, showing the interactions with the hapten. Side chains are shown only for the residues that are 4 Å or less from the ligand. The light chain is shown in lavender and the heavy chain in blue (*40*).

Comparison with chorismate mutase. The recent analysis (*16*) of the 2.2 Å crystal structure of a monofunctional chorismate mutase from *Bacillus subtilis*, complexed with the same transition state analog 4 used in our study, provides an opportunity for a direct structural comparison of the enzyme and catalytic antibody binding sites (Fig. 6). The active sites of the trimeric enzyme are located at the interfaces of two adjacent subunits and make extensive hydrophobic, ionic, and polar contacts with the bound transition state analog. The transition state analog binds to the enzyme with a dissociation constant (K_i) of 3 μM (*11*), or roughly five times weaker than with 1F7 (K_i = 0.6 μM) (*3*).

Chorismate mutase and 1F7 bury an almost identical proportion (≈90 percent) of the transition state analog (182 $Å^2$), but only 213 $Å^2$ of the active site of the enzyme is buried (compared to 265 $Å^2$ for 1F7), implying a more precise fit in the enzyme-inhibitor complex. A significant difference between the complexes is that almost diametrically opposed faces of the transition state analog are buried in its interaction with the two proteins (Fig. 6). In the case of 1F7, hapten orientation was predetermined by the choice of the hydroxyl group for attachment of the carrier protein, so that the two carboxylate groups constitute the dominant recognition elements. In contrast, the enzyme makes the greatest number of contacts to the carboxylate at C-11 and to the hydroxyl group at C-4. The C-10 carboxylate is located at the entrance of the active site and is largely solvent exposed.

In addition to differences in orientation of the transition state analog within the respective chorismate mutase and antibody active sites, the nature and number of the specific interactions that mediate ligand recognition in these two systems are distinct. Thus, the enzyme provides many more of the possible hydrogen-bonding interactions to the key functional groups of the hapten than does the antibody. The side chains of Arg^{7}, Arg^{90}, and Tyr^{108} are all within hydrogen bonding distance

(<3.3 Å) of the carboxylate at C-11, whereas the side chains of Glu[78] and Cys[75] and the main chain amide of Cys[75] appear to interact with the hydroxyl group at C-4 (*16*). Moreover, the enzyme has a larger number of charged residues than the antibody has for hapten binding, including two positively charged arginines and a negatively charged glutamate compared to the single arginine residue in the antibody active site. Because the oxabicyclic core of **4** is neutral, proximity to the extra positive charge may destabilize the enzyme-hapten complex somewhat and account for its larger dissociation constant relative to the antibody-hapten complex. It is noteworthy that the carbocyclic analog of **4** (in which the ether oxygen has been replaced with a methylene group) is roughly 250 times less potent as an inhibitor of the *Escherichia coli* chorismate mutase-prephenate dehydrogenase (*30*).

Mechanistic implications. As noted by Knowles and co-workers (*10*), a protein might accelerate the conversion of chorismate into prephenate by various mechanisms (Fig. 7). For example, as discussed above, a significant rate advantage can be expected simply from effective utilization of binding energy by the enzyme to fix the flexible substrate firmly in the requisite pseudodiaxial conformation, and to freeze out rotational degrees of freedom in the transition state (*31*). A cationic substituent effect could also speed up the concerted reaction: Model studies (*32*) have suggested that species like **5**, arising from transient protonation and ionization of the C-4 hydroxyl group by the enzyme, would undergo rapid sigmatropic rearrangement. The enzyme might also provide low-energy alternatives to the concerted process, involving, for example, heterolytic cleavage of the bond between the ether oxygen and C-5 followed by S_N2' attack of the enol pyruvate moiety at C-1 of the cyclohexadiene ring (*10*). Provision of a proton to the enolpyruvate as in **6**, or nucleophilic assistance by an appropriately positioned enzymic group, as in **7**, would favor such a pathway.

The structural data show that both the antibody and the enzyme (*16*) provide environments that are complementary to the conformationally restricted transition state analog and, by inference, to the transition state for the concerted rearrangement. There are no functional groups near the transition state analog in either active site (Figs. 5 and 6) that could form a covalent intermediate with the substrate (through C-5), or participate in general acid-base catalysis. This assessment is fairly robust in the case of the antibody, as the nearest carboxyl groups (Asp[H52] and Asp[H97] side chains) are both 8.2 Å from the transition state analog, and the nearest serine hydroxyl group (Ser[L51]) is 10.5 Å away; all of these distances are in excess of the 0.3 to 0.5 Å estimated error of the model coordinates (*24*). In the case of the enzyme, the only potential nucleophile (Cys[75]) appears to be too far from C-5 (≈5 Å) to participate directly in catalysis. Therefore, both the enzyme, as noted by Lipscomb and co-workers (*16*) and others (*11*), and the antibody apparently catalyze the isomerization of chorismate by stabilizing the same pericyclic transition state that occurs in the uncatalyzed thermal reaction, rather than by providing alternative pathways to the product.

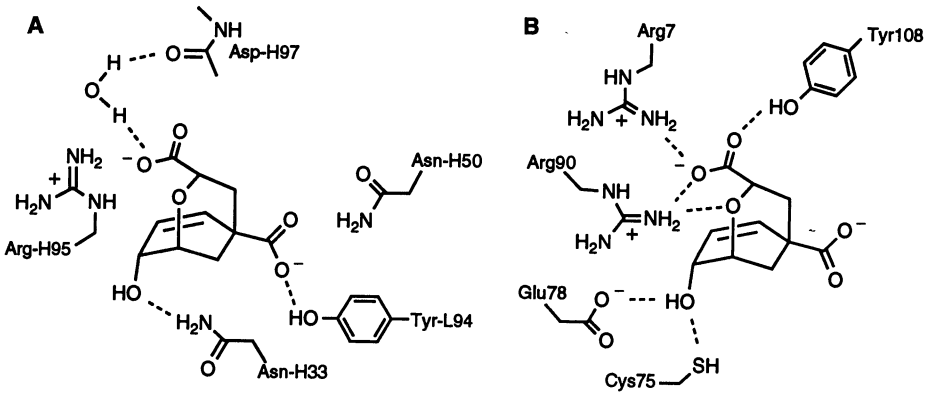

Fig. 6. Schematic diagram comparing the hydrogen bonding and electrostatic interactions of the transition state analog with relevant side chains of 1F7 (**A**) and *B. subtilis* chorismate mutase (**B**) (*16*). Dashed lines indicate hydrogen bonds. Bonds are not indicated for residues at distances greater than 3.3 Å from the ligand.

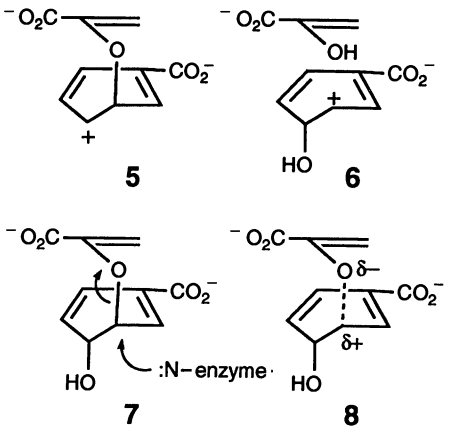

Fig. 7. An illustration of several mechanistic possibilities for the rearrangement of (−)-chorismate to prephenate, including carbocation formation at C-4 (**5**), protonation of the ether oxygen [**6**], and nucleophilic attack at C-5 (**7**). Structure **8** represents the putative dipolar transition state for the concerted pericyclic reaction.

Preorganization of the substrate into a reactive conformation is thus likely to contribute to catalysis. In the absence of a major rearrangement of the combining site of the antibody, only the pseudodiaxial conformer of chorismate would be readily accommodated within the binding pocket. The structural evidence is thus consistent with NMR data (*15*), an indication that the predominant fraction of antibody-bound (−)-chorismate is in a diaxial conformation. Although some conformational flexibility is possible (arising perhaps from small rotations about the bond connecting C-5 and the ether oxygen of the substrate), the shape complementarity between the transition state analog and the antibody binding site would appear to preclude binding of the extended pseudodiequatorial conformations of either the substrate or the product. Similar conclusions have been inferred from the structure of chorismate mutase (*33*).

While the active sites of both 1F7 and chorismate mutase are configured to bind the diaxial conformer of chorismate preferentially, the two proteins achieve this end by distinctly different means (Fig. 6). The common element seen in the two structures is binding of selected functional groups of the hapten, which causes the enol pyruvate side chain to be fixed in the requisite axial position over the cyclohexadiene ring. In 1F7, these are the carboxylates and the hydroxyl group, whereas in chorismate mutase the principal binding points are the C-11 carboxylate and the hydroxyl group. The difference in the relative orientation of the transition state analog in the enzyme and antibody binding sites could be interpreted as the main source of difference in their catalytic efficiency (a factor of $\approx 10^4$ times). However, the same transition state analog, also linked through the hydroxyl group, has been used to select an antibody whose activity is only 100 times lower than that of chorismate mutase (*4*), suggesting that recognition of the enol pyruvate side chain and at least one of the functional groups on the ring may be sufficient for high rates.

Although both proteins make interactions with the transition state analog that would be suitable for constraining the flex-

ible substrate and stabilizing the transition state, several factors may account for their differences in catalytic potency. Efficient catalysis requires that the transition state of the reaction be stabilized to a greater extent than the bound ground state, and interactions optimized (by the immune system) for high-affinity binding of the imperfect transition state analog are unlikely to be optimized for stabilizing the true metastable species. The putative water-bridged hydrogen bond that fixes the C-11 carboxyl group of **4** to the antibody main chain, for example, may not be as effective at immobilizing the enol pyruvyl side chain in the transition state as the multiple hydrogen bonding and electrostatic interactions provided by the natural enzyme for the same purpose (Fig. 6). Greater difficulty in fully restricting the rotational degrees of freedom of the transition state in the antibody combining site may account, in part, for the large differences in activation entropy that have been observed for these systems.

Studies of the uncatalyzed concerted rearrangement of chorismate (*7*, *13*) have indicated that the transition state is highly polarized (**8**), raising the additional possibility that the enzyme and the antibody may differ in their ability to stabilize this dipolar transition state electronically. In the enzyme, the guanidinium group of Arg^{90} is reasonably positioned at 3.1 Å from both the C-11 carboxyl group and the ether oxygen of the hapten (*16*) for electrostatic stabilization of the partial negative charge that develops on the ether oxygen. Similarly, the negatively charged carboxylate side chain of Glu^{78} might complement the partial positive charge that develops on the cyclohexadiene ring (*33*). Any ground state destabilization resulting from juxtaposition of apolar portions of the substrate with these ionic residues may be relieved at the transition state. In 1F7, the guanidinium group of Arg^{H95} may play a similar role as Arg^{90} on the enzyme (Figs. 5 and 6). It is only 4.2 Å from both the C-11 carboxyl group and the ether oxygen of the hapten, and might interact with the ether oxygen of the substrate more directly following a minor conformational readjustment. However, since Arg^{H95} is also presumably important in mediating recognition of the carboxylate group on the enol pyruvate side chain, this additional interaction may limit its effectiveness at stabilizing any charge that develops on the transition state as the reaction proceeds. The antibody pocket also lacks an analog of Glu^{78} for stabilization of a transient positive charge on the cyclohexadienyl ring.

The differing electronic features of the enzyme and the antibody active sites can be easily rationalized on the basis of hapten structure. The Arg^{H95} interaction was presumably elicited by the negatively charged C-11 carboxyl group of **4**, but the hapten lacks positively charged groups that would favor selection of a counterpart to Glu^{78} of the enzyme. Thus, despite its net shape and electrostatic complementarity to the transition state analog, 1F7 provides at most one of the two specific interactions that might fully stabilize a dipolar transition state. A compound like **9**, containing an ammonium ion in place of the C-4 hydroxyl group, might be expected to be a more potent inhibitor of the natural enzyme because of more complete charge complementarity. If coupled through its C-10 carboxyl group for immunization, compound **9** could yield antibodies that better mimic the properties of the *B. subtilis* enzyme.

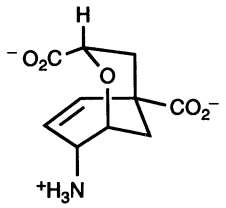

9

Although transition state analog binding to the natural enzyme is accompanied by only minimal conformational changes of protein residues (*16*), movement of the Arg^{H95} side chain in the antibody is probably required for substrate binding and product release because this residue partially blocks access to the binding site from solvent. Insofar as it makes different interactions with substrate, transition state, and product, and is required for catalysis, its rearrangement might contribute to the unfavorable entropy of activation associated with the 1F7-catalyzed reaction. Precedent for ligand-dependent conformational changes in antibody binding sites, ranging from side chain and loop movements to domain rearrangements, can be found in a number of antibody-antigen complex structures (*26*, *28*, *34*).

Future development of catalytic antibodies. Comparison of the structure of the 1F7-hapten complex with the highly evolved chorismate mutase from *B. subtilis* illustrates that the differences in van der Waals and charge complementarity to the transition state analog in these two systems may merely be matters of degree, and may fall short of defining an essentially different mechanism for the enzyme versus the antibody.

The degree to which the hapten design is mirrored by the structure of the resulting antibody combining site is of interest. The 1F7 binding site, selected to recognize the shape and ground-state electrostatic character of a conformationally restricted transition state analog and bind it with high affinity and specificity, appears to fulfill this role fairly well. The goal of distinguishing and selecting the reactive conformer of chorismate from a mixed population of conformers in solution has been achieved (*15*), as has a high degree of enantioselectivity (*3*). However, any dipolar character of the transition state, which was not effectively modeled by the hapten, would seem to be correspondingly less favored by the antibody. This is made clear by comparison with *B. subtilis* chorismate mutase, which seems to make more effective electrostatic interactions with the transition state analog. It would appear that additional strategies might be required to enhance those features of the hapten that do not effectively mimic the characteristics of the actual transition state.

The faithfulness with which the chemical nature of the transition state analog has determined the properties of the catalytic antibody indicates that further development of this and similar protein catalysts is amenable to a rational approach. The fact that another catalytic antibody produced with the same transition state analog (*4*) accelerates the Claisen rearrangement at a rate intermediate between that of 1F7 and chorismate mutase suggests that antibodies are not intrinsically limited in their ability to promote this type of reaction. These results indicate that it should be possible, given improvements in transition state analog design, screening of antibodies, structure-based mutagenesis experiments, and random mutagenesis coupled with genetic selection (*35*), to create antibodies that more closely approach the efficiency of enzymes in the catalysis of concerted chemical reactions. For example, a mutation of Asn^{H33} in 1F7 to aspartate might increase the antibody-catalyzed rate acceleration by providing an additional electrostatic interaction to stabilize a positive charge at C-5 of the transition state.

The antibody does not appear to function by a dramatically different catalytic mechanism compared with that of the natural enzyme. Considered in isolation, the 1F7 Fab'-hapten complex might be viewed as irrelevant to catalysis by "true" enzymes. On the contrary, the similarities between 1F7 and chorismate mutase indicate that the same mechanisms that give enzymes their enormous usefulness are not limited to highly evolved biological systems, but are accessible to the approaches of rational design. The development of catalytic antibodies to rival the efficiency of any natural enzyme may be merely a matter of optimizing the current approach, rather than a switch to an entirely new paradigm.

REFERENCES AND NOTES

1. D. Hilvert, *Acc. Chem. Res.* **26**, 552 (1993); P. G. Schultz and R. A. Lerner, *ibid.* p. 391; J. D. Stewart, L. J. Liotta, S. J. Benkovic, *ibid.*; p. 396.

2. W. P. Jencks, *Catalysis in Chemistry and Enzymology* (McGraw Hill, New York, 1969), p. 288.
3. D. Hilvert, S. H. Carpenter, K. D. Nared, M.-T. M. Auditor, *Proc. Natl. Acad. Sci. U.S.A.* **85**, 4953 (1988); D. Hilvert and K. D. Nared, *J. Am. Chem. Soc.* **110**, 5593 (1988).
4. D. Y. Jackson *et al.*, *J. Am. Chem. Soc.* **110**, 4841 (1988); D. Y. Jackson, M. N. Liang, P. A. Bartlett, P. G. Schultz, *Angew. Chem. Int. Ed. Engl.* **31**, 182 (1992).
5. P. R. Andrews, G. D. Smith, I. G. Young, *Biochemistry* **12**, 3492 (1973).
6. H. Görisch, *ibid.* **17**, 3700 (1978).
7. L. Addadi, E. K. Jaffe, J. R. Knowles, *ibid.* **22**, 4494 (1983).
8. S. G. Sogo *et al.*, *J. Am. Chem. Soc.* **106**, 2701 (1984).
9. S. D. Copley and J. R. Knowles, *ibid.* **109**, 5008 (1987); *ibid.* **107**, 5306 (1985).
10. W. J. Guilford, S. D. Copley, J. R. Knowles, *ibid.* **109**, 5013 (1987).
11. J. V. Gray, D. Eren, J. R. Knowles, *Biochemistry* **29**, 8872 (1990).
12. P. A. Bartlett and C. R. Johnson, *J. Am. Chem. Soc.* **107**, 7792 (1985).
13. R. M. Coates, B. D. Rogers, S. J. Hobbs, D. R. Peck, D. P. Curran, *ibid.* **109**, 1160 (1987); J. J. Gajewski *et al.*, *ibid.*, p. 1170; D. L. Severance and W. L. Jorgensen, *ibid.* **114**, 10966 (1992).
14. J. L. Pawlak *et al.*, *ibid.* **111**, 3374 (1989).
15. A. P. Campbell, T. M. Tarasow, W. Massefski, P. E. Wright, D. Hilvert, *Proc. Natl. Acad. Sci. U.S.A.* **90**, 8663 (1993).
16. Y. M. Chook, H. Ke, W. N. Lipscomb, *ibid.*, p. 8600.
17. M. R. Haynes, E. A. Stura, D. Hilvert, I. A. Wilson, *Proteins* **18**, 201 (1994).
18. P. M. D. Fitzgerald, *J. Appl. Crystallogr.* **21**, 273 (1988).
19. A. T. Brunger, J. Kuriyan, M. Karplus, *Science* **235**, 458 (1987); A. T. Brunger, *J. Mol. Biol.* **203**, 803 (1988). The X-PLOR topology and parameter files used were toph19x.p.pro and param19x.pro, respectively.
20. Y. Harada, A. Lifchitz, J. Berthou, *Acta Crystallogr.* **A37**, 398 (1981).
21. T. A. Jones, *J. Appl. Crystallogr.* **11**, 262 (1978).
22. A. Hodel, S.-H. Kim, A. T. Brunger, *Acta Crystallogr. A* **48**, 851 (1992).
23. R. A. Laskowski, M. W. MacArthur, D. S. Moss, J. M. Thornton, *J. Appl. Crystallogr.* **26**, 283 (1993).
24. V. Luzzati, *Acta Crystallogr. A* **5**, 802 (1952).
25. D. R. Davies, E. A. Padlan, S. Sheriff, *Annu. Rev. Biochem.* **59**, 439 (1990); E. A. Kabat, T. T. Wu, *J. Immunol.* **147**, 1709 (1991).
26. I. A. Wilson and R. L. Stanfield, *Curr. Opin. Struct. Biol.* **3**, 113 (1993).
27. The buried surfaces were calculated by means of the program MS [M. L. Connolly, *J. Appl. Crystallogr.* **16**, 548 (1983)] with 1.7 Å probe radius.
28. R. L. Stanfield, T. M. Fieser, R. A. Lerner, I. A. Wilson, *Science* **248**, 712 (1990); J. M. Rini, U. Schulze-Gahmen, I. A. Wilson, *ibid.* **255**, 959 (1992).
29. The decision was made to introduce a water molecule into the refinement at this position on the basis of the resulting improvements in the electron density in this region, and in the main-chain geometry at Asp^{H97}. In F_o-F_c omit maps, electron density for the water molecule was apparent at contour levels ≤ 3.3 σ. The placement of water molecules in a structure at this moderate resolution was subject to significant uncertainty, and must be regarded as provisional pending structural information at higher resolution.
30. P. A. Bartlett, Y. Nakagawa, C. R. Johnson, S. H. Reich, A. Luis, *J. Org. Chem.* **53**, 3195 (1988).
31. F. H. Westheimer, *Adv. Enzymol. Related Areas Mol. Biol.* **24**, 441 (1962); W. P. Jencks, *ibid.* **43**, 219 (1975).
32. C. J. Burrows, B. K. Carpenter, *J. Am. Chem. Soc.* **103**, 6983 (1981); R. Breslow and J. M. Hoffman, *ibid.* **94**, 2110 (1972).
33. Y. M. Chook and W. N. Lipscomb, personal communication.
34. R. L. Stanfield, M. Takimoto-Kamimura, J. M. Rini, A. T. Profy, I. A. Wilson, *Structure* **1**, 83 (1993); D. R. Davies and E. A. Padlan, *Curr. Biol.* **2**, 254 (1992).
35. Y. Tang, J. B. Hicks, D. Hilvert, *Proc. Natl. Acad. Sci. U.S.A.* **88**, 8784 (1991).
36. B. W. Matthews, *J. Mol. Biol.* **33**, 491 (1968).
37. S. C. Harrison, *J. Appl. Crystallogr.* **1**, 84 (1968).
38. A. J. Howard *et al.*, *ibid.* **20**, 383 (1987).
39. Prepared by R. Stanfield using MCS [M. L. Connolly, *J. Mol. Graphics* **3**, 19 (1985)].
40. Prepared by M. Pique as in [C. Upson *et al.*, *IEEE Computer Graphic Appl.* **9**, 30 (1989)].
41. We thank J. Arevalo, D. Fremont, D. Jewell, R. Stanfield, and T. Yeates for advice; R. Stanfield for Fig. 3 with software written by M. Sanner; M. Pique for Figs. 4 and 5; M.-T. M. Auditor and G. Fieser for technical assistance; and R. Lerner for constant support and encouragement. We are indebted to W. N. Lipscomb and Y. M. Chook for providing the coordinates of the chorismate mutase structures (Brookhaven Protein Data Bank references 1CHS and 1CHT). Supported by NIH grants AI-23498 (I.A.W.) and GM-38273 (D.H.), American Cancer Society grant FRA-60465 (D.H.), and The Scripps Research Institute graduate program (M.R.H.). This is publication No. 8258-MB from The Scripps Research Institute. Coordinates have been deposited in the Brookhaven Protein Data Bank.

17 November 1993; accepted 7 January 1994